Macromolecules
ARTICLE

Macromolecules **2010**, *43*, 4201–4209 **4201**
DOI: 10.1021/ma100217q

Extraction of Microfibrils from Bacterial Cellulose Networks for Electrospinning of Anisotropic Biohybrid Fiber Yarns

Richard T. Olsson,*,‡ Roland Kraemer,‡ Amparo López-Rubio,† Sergio Torres-Giner,† María José Ocio,† and José María Lagarón†

†*Novel Materials and Nanotechnology, Institute of Agrochemistry and Food Technology, CSIC, Apartado Correos 73, 46 100 Burjassot (Valencia), Spain, and* ‡*School of Chemical Science and Engineering, Fiber and Polymer Technology, Royal Institute of Technology, SE-100 44 Stockholm, Sweden*

Received January 28, 2010; Revised Manuscript Received March 30, 2010

ABSTRACT: Electrospinning of uniform biohybrid fibers with concealed cellulose microfibrils (CMF) is reported as a promising and environmentally sound concept for reinforcement of polymer nonwoven fiber systems of fine dimensions. The extraction and refinement of the high-strength crystalline microfibril bundles (15−20 nm thick) from bacterial cellulose networks is presented, as well as their morphology prior to and post electrospinning, Nanofibers composed of a poly(methyl methacrylate) (PMMA) matrix with cellulose contents reaching 20 wt % were repeatedly obtained. A high degree of dispersion of the microfibrils was obtained for a variety of CMF contents and the aggregation of the CMF was greatly suppressed as the microfibrils were aligned and rapidly sealed inside the acrylate matrix during the continuous formation of the fibers. The limited CMF aggregation up to 7 wt % was related to a suppressed phase separation caused by the rapid solidification of the polymer solutions during spinning. The fibers' diameters decreased significantly from ∼1.8 μm (1 wt %) to ∼100 nm (20 wt %) with increasing cellulose contents, resulting in CMF agglomerations and percolating architectures within the acrylate host, which was consistent with microscopy, thermogravimetric analysis (TGA), and differential scanning calorimetry (DSC) evaluations. The nominal content of cellulose in the fibers was assessed by Lorentzian profile fit assignment of the crystalline vs amorphous fractions of the fibers' X-ray diffractograms. TGA of fibers with low CMF content revealed that both CMF and PMMA showed a significantly improved thermal stability in the composite material. The biohybrid fibers were continuously aligned into an anisotropic nanocomposite yarns from a liquid support during spinning. The strategy described herein may allow for new mechanically robust nonwoven fiber systems, or be used as implemented on existing electrospun formulations that are lacking mechanical integrity. It is envisioned that the cellulose microfibrils may be of importance in biomedical applications where biocompatibility is a requirement.

1. Introduction

The electrospinning technique has recently received attention as a versatile and potential high-throughput method to continuously process thin solid fibers from solutions[1−4] into materials aimed at applications in composites,[5] textiles,[6] filtration,[7] sensors,[8] tissue-engineering scaffolding[9] and wound dressings.[10] A variety of nonwoven fiber materials have been presented but so far most of the materials show limited strength (< 20 MPa), i.e., sensitivity to external stress due to the fine fiber dimensions.[11−15] Although the nonwovens can be cross-linked or annealed for improved mechanical performance, this leads to an unwanted reduced interactive surface area of the fibers and intrinsic reinforcement of the fiber cores is preferred.[16−18] Elongated nanoparticles has been suggested as reinforcement agents and electrospinning was demonstrated efficient for aligning rodlike particles within fibers, parallel with the main fiber axis.[19−22] As the polymer−solid solution emerge from the spinneret, the solids are within a very short time frame locked (encapsulated) in their polymer host, simultaneously as their "carrier" solution rapidly evaporates due to the large surface area of the created fibers.[23] The anisotropic particle arrangement may allow for unidirectional stress transfer to the elongated particles provided the interface between the polymer and the particles is favorable, the particle distribution uniform, and the processing conditions allows formation of uniform fibers.[24−26]

In this article, we demonstrate that microfibrils from cellulose show potential to become a novel reinforcement candidate in electrospun polymer fiber systems and we show for the first time that uniform fibers can be electrospun over a range of different microfibril concentrations. Modulus values in excess of 100 GPa have been reported for cellulose microfibrils and their mechanical strength may exceed 7−8 GPa.[28−32] In addition, the microfibril dimensions match many of currently reported electrospun fiber systems and the hydroxyl functional surface[33,34] offers potential for surface engineering to modify their physiochemical interaction with polymer host materials.[35−38] Microfibril suspensions were so far mostly processed into nanocomposite films by casting procedures, causing isotropic in-plane orientation of the microfibrils inside polymer matrices.[39,40] The benefit with casting relates to their handling in wet/dispersed state (post source extraction) with preserved crystallinity and that the microfibrils can be processed with limited irreversible agglomeration from inter microfibril condensation reactions.[41−43] However, in most nanocomposite preparation methodologies, microfibril interactions have proven unavoidable and in the majority of thermoplastic polymers the hydrophilic surface of the microfibrils causes detrimental phase separation and agglomeration.[44−47] Agglomeration

*Corresponding author. E-mail: richard@polymer.kth.se.

Published on Web 04/07/2010

may relate to insufficient solubility of the microfibril surface in the polymer host matrix, but also to the significant time span necessary for the solvent to evaporate during casting procedures, thus allowing phase separation to readily appear.

The few reports concerning electrospinning of microfibril containing fibers were either restricted to very low contents of microfibrils (< 0.5 wt %)[48] or relied in the use of compatibilizers to improve the microfibril−host matrix compatibility to favor formation of uniform fibers for a limited number of compositions.[49] Unfortunately, relatively little attention was devoted to the characteristics and the handling of the microfibrils prior to the electrospinning, which was experienced fundamental for the outcome of the results reported herein. We therefore place an emphasis on the extraction of the microfibrils from one of its biological sources (bacterial cellulose) and the morphological characteristics of the microfibrils prior to and post electrospinning. This source of the microfibrils was primarily selected due to the high crystallinity of bacterial cellulose and the absence of cell wall polymers present in wood fibers, but also due to its readily availability as low cost material from Asian agricultural industry.[50−52] By a solution exchange procedure, we introduce the microfibrils into a mixed solvent suitable for electrospinning microfibril−PMMA hybrid fibers, omitting drying of the microfibrils in order to prevent agglomeration. We demonstrate that it is possible to electrospinn uniform fibers (approximate thickness: 0.1−1.4 μm) with contents as high as 20 wt % of cellulose microfibrils distributed in the hybrid fibers and that the microfibrils align parallel inside/along the longitudal axis of the hybrid fibers. We also show that microfibrils exhibit improved thermal stability as sealed inside the polymer matrix, while the degradation of the matrix polymer is shifted to higher temperatures. Finally, we demonstrate that the electrospun hybrid fibers can be aligned into anisotropic nanocomposite yarns and how the nominal contents of incorporated microfibrils can be assessed by X-ray diffraction. Cellulose microfibrils will from hereon be designated the abbreviation CMF.

2. Experimental Section

2.1. Bacteria and Chemicals. *Gluconacetobacter xylinus* (ATCC 23767) was used to grow cellulose mats from a modified Hestrin/Shramm medium. The medium was composed of (per liter of distilled water): 20 g of D-glucose (Laboratorios Conda, Pronadisa, Micro & Molecular Biology, Cat. 1900), 5 g of yeast extract (Laboratorios Conda, Pronadisa, Micro & Molecular Biology, Cat. 1702.10), 1.15 g of anhydrous citric acid (reagent grade, Scharlau), 5.7 g of magnesium sulfate (puriss, p.a., Fluka), and 12.25 g of triphosphate water (TPW) from Scharlau (5.0 g of peptone, 2.5 g of sodium chloride, 4.5 g of disodium phosphate, and 0.75 g of potassium phosphate). A 1 vol % aliquote of ethanol (96%) was used to enhance the cellulose production. The medium was sterilized in an autoclave for 20 min at 121 °C and cooled to room temperature before use.

2.2. Cellulose Fiber Synthesis. The bacteria were inoculated in a 2 mL sample of the growth medium. After 3 days, the 2 mL solution with bacteria and cellulose was reinoculated into a larger volume of 200 mL of growth medium. This solution was further reinoculated into 2 L of growth medium, which finally was used to inoculate 20 L of medium. The initial pH of the 20 L medium was 5.7 and the culture started to generate uniform mats of cellulose after 2 days. After 7 days of growth at 24 °C, a mat was harvested. The weight of a wet mat was approx 1.0 kg (including the growth medium), equivalent to 9.2 g of dry cellulose.

2.3. Cellulose Refining and Microfibril Extraction. A 1.0 kg cellulose mat was cut into smaller pieces (4 cm × 4 cm × 1 cm) and washed thoroughly to remove the growth medium by boiling it several times in distilled water. When no odors or color of the growth medium inside the cellulose mat could be detected, the cellulose pieces were boiled for 2 × 20 min in a 1.5 L aqueous solution of 10% v/v concentrated NaOH (Ph. Eur., Panreac Quimica Sau) and finally washed in distilled water until neutral pH was obtained. The pieces were compressed into thin sheets to exclude most of the water and then added to 1 L of a 50% v/v aqueous solution of sulfuric acid (95−97%, Sigma-Aldrich). The solution was stirred for 72 h at 60 °C until no visible pieces of cellulose were apparent. The solution was isothermally centrifuged at 15 °C and 24 000 rpm three times for 20 min. Between each centrifugation cycle, the cellulose was collected at the bottom of the centrifuge tubes and the acidic supernatant was decanted and replaced with 750 mL distilled water. After the third cycle of centrifugation, a neutral pH was obtained and the supernatant was transparent. The cellulose microfibrils (CMF) were re-dispersed using a high-shear mixer (Ultra Turrax DI-25) for 5 min between each centrifugation. A sample of the final aqueous suspension of fibrils was taken and is shown in Figure 1. The water of the CMF suspension was replaced by 0.75 L of acetone, which was further replaced by 0.75 L of 50/50 vol./vol % DMF/THF solvent in the same manner as the acid was removed post hydrolysis. The concentration of fibrils was determined as 1.9 ± 0.1 wt % after evaporation of DMF/THF solution at −100 kPa pressure (80 °C) for two separate samples.

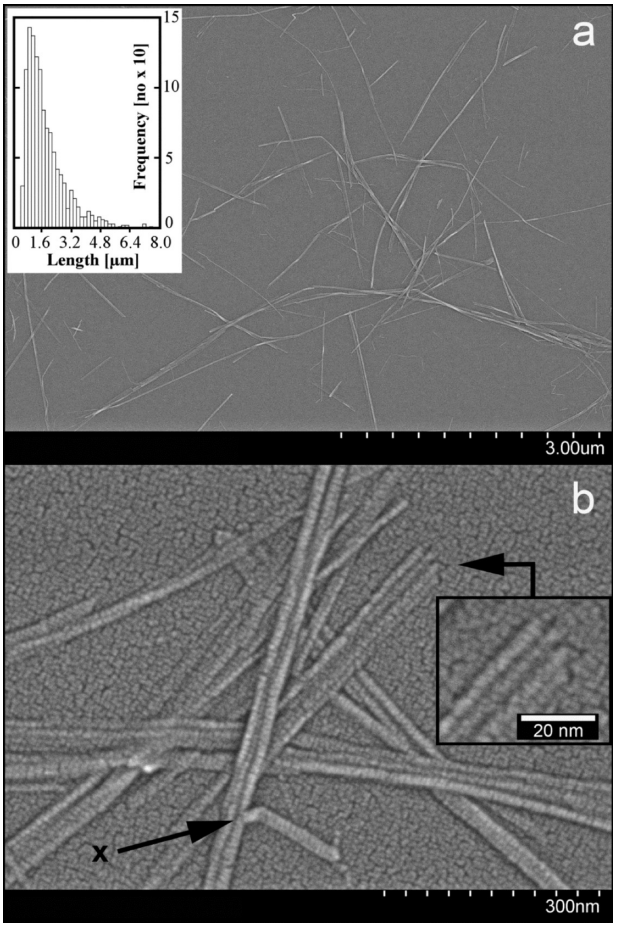

Figure 1. (a) Microfibril bundles extracted from bacterial cellulose network grown by *Gluconbacter xylinum* (ATCC 23767), extracted by acidic hydrolysis, and adsorbed from a ca. 0.01 wt % aqueous suspension, inset shows their size distribution. (b) High magnification of bundles of fibrils. The inset shows the edge of a bundle consisting of 4 fibrils. The arrow highlights a kink (x) revealing the thin whisker's morphology. Dotted pattern is the gold/palladium coating of 1−2 nm thickness.

2.4. Preparation of Solutions for Electrospinning. The refined solution of microfibrils in DMF/THF was diluted to twice its

Table 1. Preparation of Solutions for Electrospinning

	R1	NC1	NC3.5	NC7	NC14	NC20
PMMA powder (g)	2.06	17.58	4.90	2.36	1.09	0.71
CMF−DMF/THF (g)		18.50	18.50	18.50	18.50	18.50
DMF/THF (g)	18.50	120	30	10	4	
CMF/PMMA to DMF/THF (%)	10.0	12.8	10.5	9.0	5.9	4.6
CMF to PMMA (wt %)	0	1.0	3.5	7.0	14.0	20.0

The concentration of microfibrils ranged from 1 to 20 wt % with regards to dissolved PMMA polymer (NC1 to NC20). R1 is the PMMA control.

volume, resulting in a 0.95 wt % suspension of microfibrils (CMF−DMF/THF). This master solution was used to dissolve different amounts of poly(methyl methacrylate) with a mass average molar mass of 350.000 g/mol (Sigma-Aldrich) according to Table 1. To obtain solutions suitable for electrospinning, the solution viscosity was adjusted by addition of DMF/THF solvent such that uniform fibers without beads were obtained during spinning. The total content of PMMA and CMF in the DMF/THF solvent varied between 5 and 13 wt % (Table 1). The pure PMMA solution was prepared by dissolving 2.06 g of PMMA into 18.50 g of DMF/THF (50/50 vol %).

The solutions were stirred for 24 h prior to spinning and sonicated immediately before addition to the polymer reservoir using an ultrasonic horn (Sonoplus HD 2200, Bandelin). The ultrasonication was performed for 3 min at 39% of the maximum intensity in sequences of 20 s with 20 s intervals for a total duration of 6 min. The temperature of the solutions was 50 to 55 °C during the electrospinning.

2.5. Electrospinning. The polymer reservoir was a plastic syringe (5 mL) connected to a continuous feed system from kd Scientific, adjusted to a solution feed-rate of 0.30 μL/min. The solutions were directed via Teflon tubing to a blunt syringe needle with an inner diameter of 1.0 mm connected to a 30 kV power unit from Acopian. A needle to collector distance of 140 mm and a voltage of 12 kV (current output of 1 mA) were used. The collector was an aluminum reservoir filled with water and the fibers were collected on the surface of the water 120 mm from the needle tippet. The spinning was performed under air, 40% RH, 21 °C.

2.6. Microscopy, X-ray, and Thermogravimetric Analysis. Scanning electron microscopy (SEM) was conducted on a Hitachi S-4100 or Hitachi S-4800 microscope using accelerating voltages of 2 kV to 10 kV. The CMF was adsorbed from an aqueous suspension ca. 0.01 wt % CMF on a silicone oxynitride chip pretreated by a PEI (M_w = 60 000, 50% aqueous, Acros Organics) solution (100 mg/L, 10 mM at pH 7) and briefly rinsed by Milli-Q water prior to immersion in the CMF suspension followed by subsequent drying. The samples were sputtered (60 s for electrospun fibers and 15 s for the adsorbed microfibrils) using an Agar high resolution sputter coater (model 208RH) equipped with a gold−palladium target and an Agar thickness monitor control unit. Wide-angle X-ray experiments (WAXS) were performed on a Siemens D5000D. Radial scans of intensity versus scattering angle (2θ) were recorded at room temperature in the angular range of 4° to 28° (2θ) (step size = 0.02°, scanning rate = 4 s/step) by using filtered Cu Kα radiation (λ = 1.54 A), an operating voltage of 40 kV, and a filament current of 30 mA. To calculate the plane d spacing Bragg's law ($\lambda = 2d \sin\theta$) was applied. Crystal size was estimated using the Debye−Scherrer formula ($d = 0.9 \times \lambda/\text{fwhm} \times \cos\theta$) and peak parameters were determined by deconvolution of the experimental diffractogram with Lorentzian profiles. The samples were prepared by compressing the electrospun fibers into round 10 mm in diameter washers, 0.2 ± 0.01 mm thick, by a commercial Specac press. Thermogravimetric analysis (TGA) measurements with heating rates of 5 °C/min were performed on a thermogravimetric analyzer (TGA/SDTA 851e, Mettler Toledo) by heating 2.8 ± 0.2 mg samples in 70 μL alumina crucibles under nitrogen. Differential scanning calorimetry (DSC) measurements were performed on a Perkin-Elmer DSC (DC7) using a heating rate of 10 °C/min under nitrogen for 8.0 ± 0.4 mg samples.

3. Results and Discussion

3.1. Cellulose Microfibrils prior to Electrospinning. Figure 1 shows the extracted CMF (microfibril bundles) adsorbed on the surface of a positively charged silicone oxynitride chip in a similar fashion as Aulin et al. adsorbed pulp derived micro fibrillated cellulose (MFC) from aqueous suspensions.[53]

Complete disintegration of microfibril bundles into individual microfibrils was not achieved within 72 h of acidic hydrolysis and mostly the fibrils remained in their natural state as bundles, shown in Figure 1, parts a and b. The bundles adsorbed as readily dispersed strands from the aqueous suspension, which is explained by electrostatic repulsion between bundles in the aqueous suspension due to the negatively charged sulfate groups induced on the surface of microfibrils during the extraction procedure.[54,55] The lateral dimensions of the bundles were approximately 15−20 nm, whereas the length varied between 0.3 and 8 μm (average ∼1.2 μm), see inset in Figure 1a. The edge of a bundle (inset Figure 1b) shows the typical configuration of the individual microfibrils inside the bundles. The bundles consisted of 3−6 microfibrils held by more than electrostatic forces since all bundles showed a similar microfibril arrangement, likely due to the presence of small amounts of paracrystalline matrix holding the microfibrils together.[42] It needs to be emphasized that the individual microfibrils show different diameters as dependent on their natural source and occasionally bundles appear to be mistaken for the individual microfibrils due to limited microscopy resolution. The microfibril diameters however are well established: for the plant parenchyma ∼2−3 nm,[56] wood sources ∼3−4 nm,[57] bacterial cellulose ∼4−7 nm,[58,59] and cotton linters and ramie ∼7−9 and ∼10−15 nm,[60] respectively. Marine resources typically yield microfibrils with larger diameters; tunicate marine animals ca. 20 nm,[27] whereas algae contain 10−70 nm wide microfibrils.[61,62] This unique characteristic allows the diameter of the microfibrils to be selectively chosen with regards to the aimed diameters of the electrospun fibers.

The width of the individual microfibrils was approximately 3−6 nm (Figure 1b, inset), which is consistent with earlier investigations on microfibrils from bacterial cellulose, whereas their length was at least 300 nm. The individual microfibrils had a whisker-like morphology with a smaller thickness than width, as described by Ohad et al.[63,64] This feature occasionally allowed the fibrils to fold/twist over their axis, possibly in the direction of their smaller thickness as indicated by an x in Figure 1b. In general, the dimensions of the bundles were similar in size to microfibrils derived from cotton or wood but shorter than microfibrils from tunicates.[65,66] The morphology of the bundles being well-defined and straight-edged, with uniform lateral dimensions, resembles more the microfibrils derived from tunicates than those derived from cotton or wood. However, the specific morphology of the microfibrils is affected by the extraction procedure, and currently procedures yielding only the individual microfibrils have not been reported for the bacterial cellulose source due to difficulties in selectively extracting the microfibrils without partial carbonization and degradation of some microfibrils. This is a consequence of an uneven dissolution of the amorphous segments holding the microfibrils in their source cellulose matrix, thus allowing some

crystalline fragments to more extended hydrolysis and possibly thermal degradation.[67,68] In general, the cellulose microfibril bundles can be considered as highly crystalline after acidic hydrolysis and the extraction of microfibrils from bacterial cellulose was a fast and straightforward process, with the benefit of no need for refinements such as dialysis and filtration of the centrifuged solutions after the hydrolysis and neutralization.[50,69] The yield of the extraction was high: 8.19 g, 89% based on the dry weight of the bacterial cellulose.

3.2. Electrospinning of Uniform PMMA−Cellulose/Microfibril Fibers. Figure 2a shows the fracture surface of fibers electrospun from a suspension containing 7 wt % microfibrils (NC7) and the fracture surface of the fibers electrospun from the PMMA solution in absence of CMF.

The microfibril bundles were evenly distributed over the fracture surface of the hybrid fibers (Figure 2a, top left), whereas a smooth fracture surface of the PMMA fibers (Figure 2a, top right) was observed. In contrast to a previous report on electrospun fibers containing CMF, the electrospun fibers did not show any microfibrils protruding the outer fiber surface.[48] The outer surface of both types of fibers showed signs of contraction around the center axis of the fibers. This rough surface morphology was possibly a result of an unbalanced evaporation of the dual phase DMF/THF solvent mixture during solidification of the fibers, as related to the higher boiling point of DMF. Rojas et al. obtained smooth fiber surfaces using solely THF as a solvent to electrospin polystyrene containing surfactant-dispersed microfibrils.[49] The formation of a wrinkled fiber surfaces has been related to the ambient conditions (humidity) during electrospinning and was attributed for polystyrene fibers electrospun from DMF solvent to a faster phase separation of the solid phase than the evaporation rate of the solvent system, whereas in the case of electropinning of micro tubular fibers (using a double coaxial capillary spinneret) the surface/shell contraction was related to the pressure drop around the fiber shell as the solvent evaporated .[70,71]

The dimensions of the fibril bundles sticking out from the fracture interfaces compared well with the dimensions of the bundles adsorbed from aqueous suspensions (compare Figures 2b and 1b). Higher magnifications revealed that all the fibrils were still in their configuration as bundles, although the microfibril PMMA suspensions were exposed to intense ultrasonication prior to electrospinning (cf. Figure 2b). The fracture surfaces of the hybrid fibers contained mostly partial pull-outs of the high-strength microfibril bundles, which may suggests limited interface adhesion. Given the high concentration of microfibrils in some of the fibers (NC7, NC14, and NC20), the average 1.2 μm length of the bundles (exceeding the fiber diameter of the spun hybrid fibers, Figures 1 and 2) and the visible parallel alignment of bundles within fracture interfaces; it is clear that the microfibrils were mostly aligned parallel with the axis of the electrospun hybrid fibers. Independent of the CMF concentration, this microfibril alignment within the hybrid fibers was found a dominant feature for all samples. In general, alignment of elongated particles in electrospun fibers have been attributed to the rapid contraction of the polymer solution emerging at the spinneret needle as the surface tension of the polymer solution was overcome and the meniscus was formed due to the high electrical field gradient. This alignment phenomenon in converging micro channels was reported for carbon nanotubes as well as *Bacillius magaterium*.[72−74] To some extent, the polarity of the crystalline microfibrils may have affected the alignment as well as the laminar flow in the solution supply hose, since elongated fillers orient in line with the direction of flow under laminar flow conditions.[75] Attempts to visualize microfibril alignment by TEM microscopy failed due to the rapid deformation of the fibers under the electron beam. It was also found impractical to uranyl acetate stain the fibers prior to the solution exchange process, possibly due to the lack of significant amorphous regions in the microfibrils.[49,76]

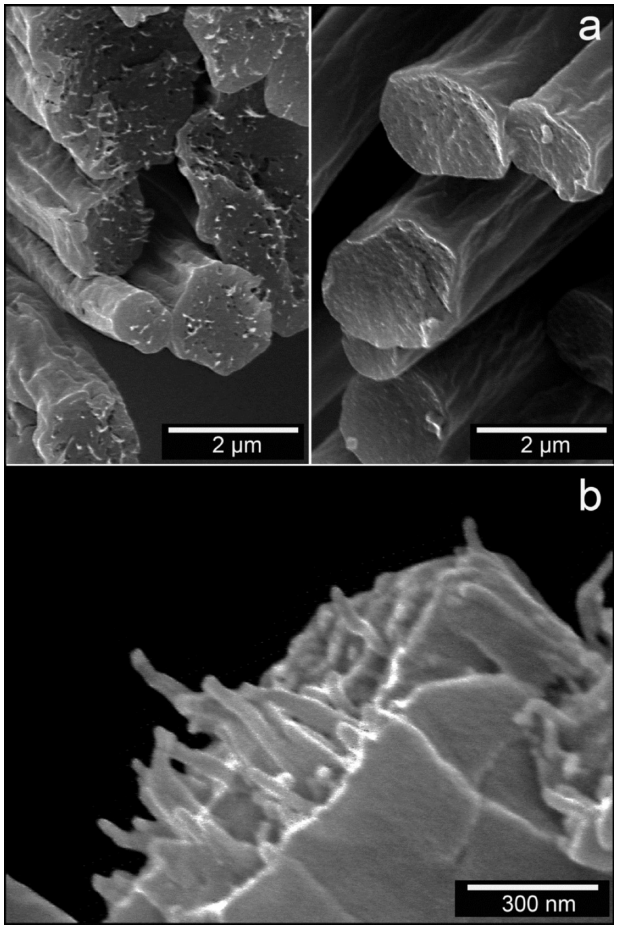

Figure 2. (a) SEM micrographs of fracture surfaces of hybrid CMF−PMMA fibers (NC7, 7 wt % CMF, top left) with cellulose microfibrils point outward from the fracture interface, and PMMA fibers (top right) with smooth fracture interface. (b) Fracture surfaces of hybrid CMF−PMMA fibers (NC14, 14 wt % CMF) showing bundles of microfibrils pointing outward form the fracture surface in parallel alignment with the hybrid fiber axis.

Figure 3 shows a selection of the different electrospun hybrid fibers containing 1, 7, and 20 wt % of microfibrils (a, b, c) and the effect of solvent dilution in terms of bead formation for the 7 wt % CMF system (d, e, f).

The electrospun fibers containing 1 wt % to 20 wt % CMF showed uniform material distribution along the longitudal direction of the fibers, see Figure 3, parts a−c. Rojas et al. obtained uniform fibers for 6 and 9 wt % CMF contents in polystyrene, using THF as solvent to electrospin polystyrene fibers containing surfactant dispersed CMF.[49] They noted that in the absence of a surfactant, the non-woven fiber mats contained beads. Such beads were absent in the uniform CMF−PMMA fiber system reported herein. However, during the evaluation of initial solution concentrations and spinning conditions, bead formation was observed; see Figure 3, parts e and f. The micrographs in the lower row show the effect of solvent dilution on CMF−PMMA with 7 wt % cellulose (NC7). The sample in Figure 3e (with bead formation) was diluted by addition of twice the mass of DMF/THF solvent, the sample shown in Figure 3f was

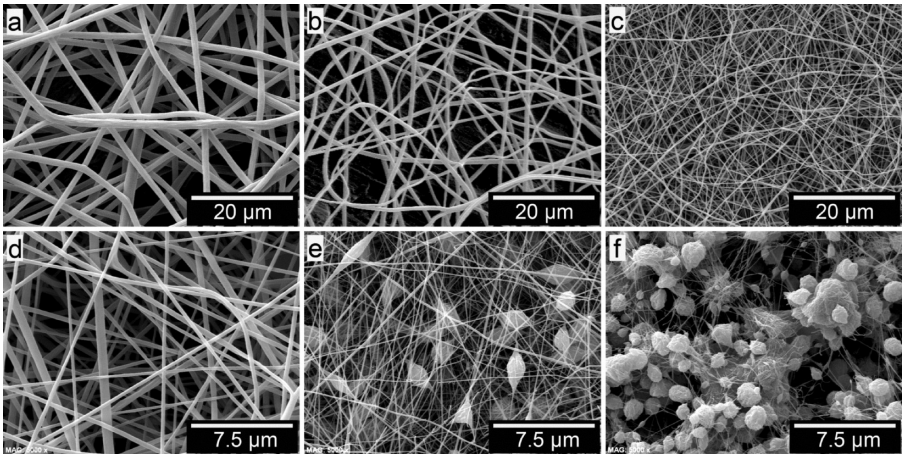

Figure 3. (Top row) Micrographs showing CMF−PMMA hybrid fibers with different contents of microfibrils: (a) 1 wt %, (b) 7 wt %, and (c) 20 wt %. (Bottom row) Micrographs showing the effect of solvent dilution on the NC7, 7 wt % CMF system: (d) NC7, not diluted, (e) NC7 with twice the mass of DMF/THF, and (f) NC7 with four times the original mass of DMF/THF.

diluted by addition of four times the mass of solvent in the original sample NC7, shown in Figure 3d. It is apparent that the beads form as the viscosity of the system decrease and a smaller content of solid material is present in the electrospinning solutions. The same effect was also observed for the 14 wt % CMF fibers. Lin et al. reported that the formation of beaded fibers was attributed to insufficient stretching of the filaments.[77] The CMF−PMMA fibers actually stretched even more in the sections between the beads. The bead formation was primarily related to capillary instability due to insufficient polymer (solids) concentration, or electric field gradient for the diluted solvent−microfibril/PMMA solutions, and as more solvent was present in the composite solutions, the thinner the fibers became between the beads, and also the frequency of the beads increased. Since the relative content of CMF toward PMMA was constant, it is suggested that the decrease in the viscosity of the solutions may also have favored a more prominent and faster phase separation (i.e., increased mobility to change phase) favoring more bead formations from the thermodynamically unfavorable solutions. This phase separation was even more apparent as a larger fraction of microfibrils with respect to PMMA was electrospun. Fibers containing 30 wt % CMF could only be electrospun immediately after ultrasonication, whereas electrospinning of fibers with 40 wt % CMF only worked sporadically and the fibers were non-uniform as a result of phase separation and flocculation of the microfibrils in the solvent phase. For all compositions, the bead formations finally converted into small spherically shaped polymer composite balls with extensive dilution, Figure 3f. A general conclusion from the solution preparation procedure was that the key to obtain uniform fibers relied on the preparation of highly concentrated solutions from CMF maintained in their suspended state after extraction, which were diluted with in increments of minimal amounts of solvent until uniform fibers were obtained.

Figure 4 shows the size distributions of only the uniform electrospun fibers and how the average fiber diameter was affected by an increasing content of cellulose microfibrils. The electrospinning parameters were identical.

A content of 1 wt % CMF resulted in thicker fibers, whereas an increase of the microfibril content yielded significantly thinner fibers and a more narrow size distribution as compared to the pristine PMMA system. The average fiber diameter of the hybrid fibers gradually decreased from ~1800 nm, s.d. 370 nm (1 wt % CMF) to ~100 nm, s.d. 25 nm

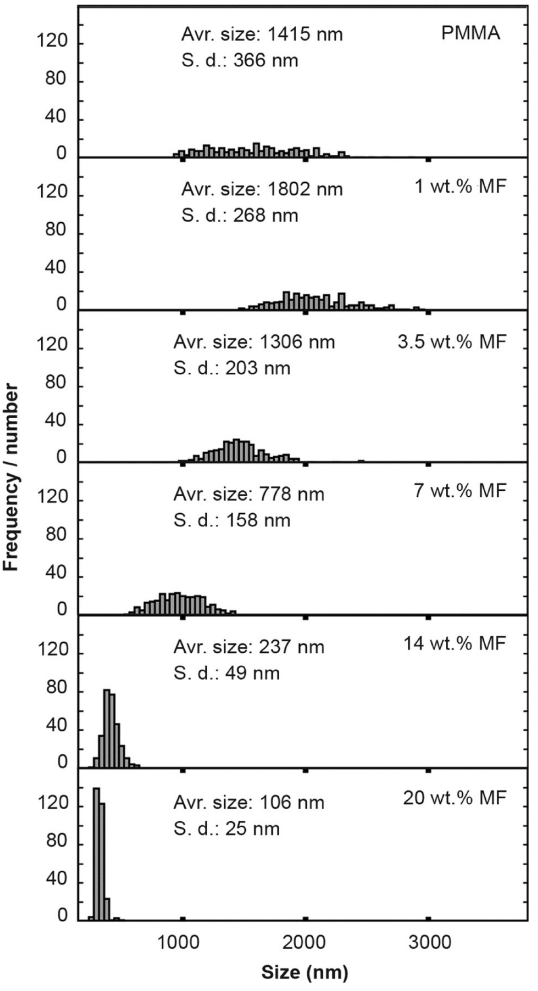

Figure 4. Size distributions of electrospun CMF−PMMA hybrid fibers with increasing contents of cellulose microfibrils. Each distribution was obtained by manual size determination of 300 fibers from SEM micrographs, using the ImageJ software.

(20 wt % CMF), whereas the average size of the pure PMMA was ~1400 nm, s.d. 370 nm. Consequently, as a reduced amount of polymer with regards to cellulose was electrospun for equivalent electrospinning parameters, the average diameter of the fibers decreased. This follows the trend that the

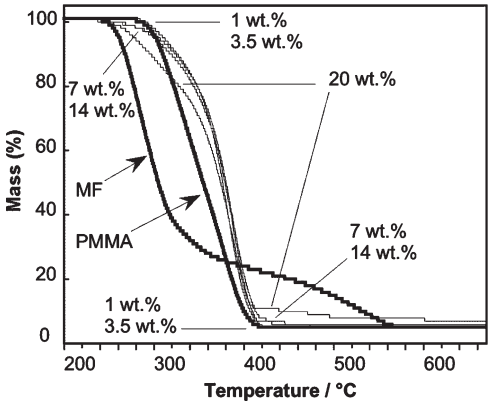

Figure 5. Thermogravimetric data for degradation for bundles of bacterial cellulose microfibrills (CMF) and PMMA (thick solid lines) and electrospun MF−PMMA hybrid fibers.

total solid contents in the electrospinning solutions decreased from 12.8 to 4.6 wt % as the CMF content increased relative to the PMMA content from 1 wt % to 20 wt %. The increase in fiber diameter for the 1 wt % CMF system (as compared to the pure PMMA system) may relate to the higher concentration of solids in the electrospun solution (12.8 wt % CMF/PMMA vs 10 wt % PMMA, see Table 1) but the exact explanation for the difference in fiber formation is still unexplored. It is suggested that the diluted 1 wt % CMF to PMMA solution is more prone to be affected by capillary effects (due to its larger contents of solids) immediately before the solutions merge from the spinneret needle or/and that the system based on solely PMMA tends to generate fibers that have been more stretched in the electrical field due to the absence of CMF.

3.3. Thermal and X-ray Analysis of Electrospun PMMA−Cellulose/Microfibril Fibers.

3.3.1. TGA and DSC Analysis. The pristine cellulose microfibrils showed an onset of degradation at 235 °C and degraded in two main steps, with maximal rates of mass loss of 264 and 515 °C, respectively, whereas the electrospun PMMA (in absence of cellulose) decomposed in two overlapping steps with an onset occurring at 274 °C and two peak mass loss rates at 310 and 352 °C. At low CMF concentrations (up to 3.5 wt %), the microfibrils of cellulose did not change the onset of degradation of the PMMA, but the mass loss was delayed and occurred in a single step at higher temperature that corresponded to the second mass loss step of PMMA (as pristine material). The contents of microfibrils in the different electrospun composite fibers could not be established by thermogravimetric analysis because the microfibrils degraded simultaneously with the surrounding PMMA matrix, Figure 5. At cellulose microfibril levels of 7 wt % and above, the onset of degradation shifted to lower temperature (Figure 5), suggesting that the cellulose forms domains of sufficient size to approach the degradation behavior found in the absence of PMMA. This trend was supported by the appearance of a small third small loss stage above 400 °C, corresponding to the high temperature mass loss of the pure cellulose. The DSC results validated the conclusions of the TG analysis, by showing a small increase in the glass transition temperature (T_g) with the inclusion of CMF up to 3.5 wt % (PMMA, 122.0 °C; 1 wt %, 125.0 °C; 3.5 wt %, 125.4 °C), whereas higher fractions of CMF showed a gradual decrease in T_g (7 wt %, 124.7 °C; 14 wt %, 124.4 °C; 20 wt %, 122.7 °C). The T_g of the 20 wt % CMF hybrid fibers showed a value much unaffected as compared to the pure PMMA, potentially because much of the CMF

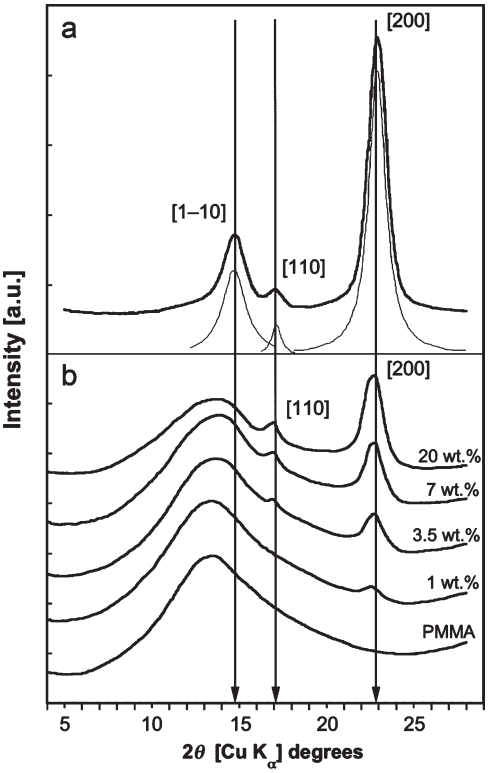

Figure 6. (a) X-ray diffraction pattern of microfibrils and the peaks related to the Lorentzian fit. Data have been offset for clarity. (b) XRD patterns of electrospun PMMA fibers and MF/PMMA hybrid fibers containing different amounts of microfibrils. Data have been offset for clarity.

were present as agglomerated bundles of fibrils and a larger fraction of PMMA was intact. A possible explanation to the reduced thermal stability for the higher end concentrations may be attributed to voids (oxygen) within the vicinity of the agglomerated microfibrils since all samples were run under nitrogen environment.[78]

3.3.2. XRD Analysis. The crystal structure of the CMF and the crystal vs amorphous phases of the hybrid fibers was analyzed using X-ray diffraction. Figure 6a shows the diffraction pattern of the extracted BC microfibrils prior to electrospinning, displaying the main peaks for cellulose I at ~14.7, 17.2, and 22.9°, corresponding to the [1$\bar{1}$0], [110], and [200] planes, respectively. The calculated crystallographic sizes according to the Scherrer equation are displayed in Table 2.

The *d*-spacing values for the crystalline microfibrils suggested that the extracted microfibrils were predominantly of the more dense and thermally stable monoclinic allomorph (I_β), which reflects that the bacterial cellulose networks were treated in NaOH and sulphuric acid at elevated temperatures during the refining and extraction of the microfibrils.[79,80] Microfibrils from bacterial cellulose in their natural state consist of two crystalline phases, i.e., triclinic (I_α) and monoclinic (I_β), whereas *d*-spacing data reflects the fractional ratio between the two phases.[81,82] The fraction of triclinic (I_α) phase often reaches values above 50% for nonthermally treated samples of bacterial cellulose.[83]

Figure 6b shows the diffractograms of the electrospun PMMA and CMF/PMMA hybrid fibers. The relative intensity of the three diffraction peaks of cellulose changed for the hybrid fibers as compared to the pristine microfibrils, as seen by the essential absence of the [1$\bar{1}$0] peak. This change in intensity was assigned to the highly ordered arrangement

Table 2. Fitting Parameters for Bacterial Cellulose Microfibril Diffraction Patterns[a]

peak	crystallographic plane	2θ [deg]	d space [Å]	width [deg]	area [au]	crystallite size [Å]
1	$1\bar{1}0$	14.69	6.02	1.65 (3)	5906 (86)	48.54
2	110	17.17	5.16	1.12 (10)	869 (67)	71.73
3	200	22.91	3.88	1.19 (1)	15597 (74)	68.11

[a] Crystallite sizes calculated in the direction perpendicular to each plane.

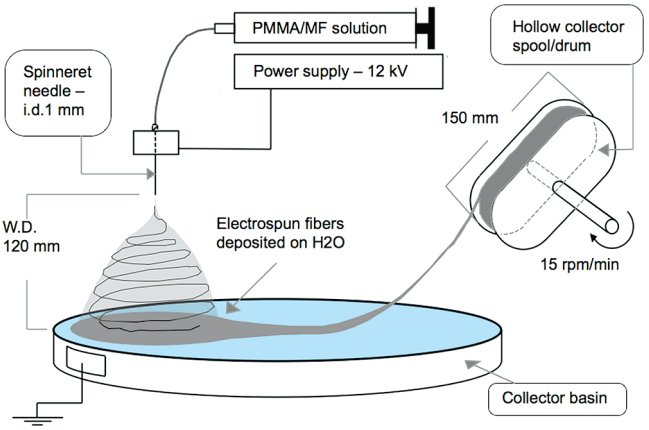

Figure 7. Electrospinning setup with a spinneret−water surface working distance of 120 mm and a spool running at 15 rpm/min. The spool (hollow) was designed to collect fibers with minimal spool−fiber yarn contact.

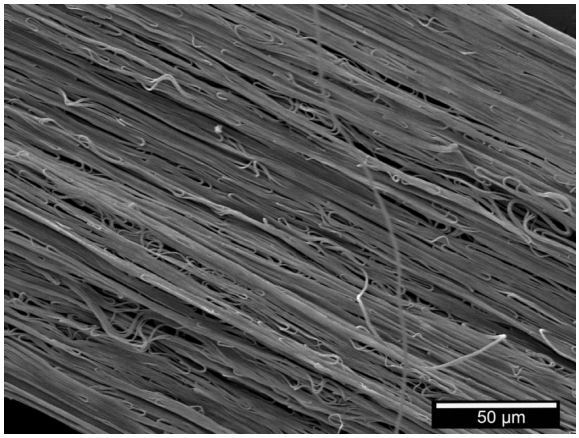

Figure 8. Aligned electrospun MF−PMMA hybrid fibers (NC7) containing 7 wt % cellulose microfibrils from bacterial cellulose.

of the cellulose microfibrils inside the electrospun fibers as well as in the compacted XRD specimen, which leads to a deflection of the [1$\bar{1}$0] plane from the detector. It follows that the ordered structure observed in SEM micrographs of a number of cross sections appropriately characterizes the hybrid fiber morphology. The whole diffraction pattern was fitted to calculate the ratio between the crystalline portions (CMF) and the amorphous content from the ratio of the integral intensity of crystalline portions to the total intensity. The ratio of the crystalline portions of the CMF hybrid fibers was linearly correlated to the mass fractions of incorporated CMF with a R^2 value of 0.991. The ratio of crystalline to amorphous parts of the XRD pattern appears thus as a straightforward method to control that the targeted amount of cellulose in the hybrid material was met.

3.3.3. Alignment of PMMA−Cellulose/Microfibril Fibers. The hybrid fibers were aligned by running the fibers over a hollow spool rotating at 15 rpm/min after the fibers were collected from a water surface, in a similar manner as E. Smit et al. collected electrospun fibers of PVDF, PVAc and PAN from a liquid static media; see Figure 7 in ref 84.

All fibers could be collected from the aqueous media, although the pristine PMMA fibers were the most fragile. The parallel alignment of the fibers on the spool resulted from the continuous action of capillary forces acting along the fibers as they were pulled through, lifted and rolled up from the water surface, Figure 8.

The obtained yarn of fibers was however not a perfectly aligned continuous system as a relative number of the kinks versus properly aligned fibers on the order of less than 1% could be determined from image analysis. Similar kinks were observed by E. Smit et al. as well as W.-E. Teo, the latter using a dynamic aqueous system to collect yarns of aligned fibers.[84,85] It appears that the alignment in liquid support systems in most cases leads to kinks that form due to the whipping and bending motions of the instable jet and result from buckling of the jet at impingement of the fibers on the deposit medium.[86] Possibly, the frequency of the kinks can be decreased by using a higher rate of collecting the fibers/yarns from the liquid media. However, many systems are limited by the low strength of the fibers that break when lifted from the liquid support if not collected as many agglomerated fibers in a yarn formation. Li et al. demonstrated that certain electrospun fiber may even break under their own weight.[87] Despite the disadvantage of the kink formation, the liquid support systems appears to be a useful method for aligning fibers on a large scale, for example for yarn applications. Aligning fibers by electrospinning onto a grounded rotating drum/mandrel has been reported as a method to obtain aligned fibers, and a sophisticated methods was presented by Carnell et al. to control the deposition of the fibers by utilizing an auxiliary negatively charged electrode.[88−91] However, this system suffers from the difficulty of adjusting the collector/drum speed as related to the flow rate of the supplied polymer solution and formation of fibers, sometimes leading to fiber stretching and necking.[92] Solid surface collection rely on developing sensitive methods to remove and transfer the fibers from the solid collector, whereas electrostatic alignment yields perfectly aligned fibers, but has so far only been demonstrated for very small samples.[93,94]

4. Conclusions

Electrospinning was used as a method to obtain uniform cellulose microfibril-PMMA fiber nanocomposites with as high as 20 wt % content of cellulose. It was found crucial to keep the microfibrils (CMF) in solution after extraction from bacterial cellulose, in order to avoid agglomeration before dispersion into the electrospinning solutions. The microfibrils were encapsulated into the hybrid CMF−PMMA fibers without signs of outer surface protrusion. Thermal characterization of the electrospun hybrid fibers indicated that the dispersion of the fiber bundles in the PMMA matrix was effective up to approximately 7 wt % CMF content, whereas higher contents showed thermal degradation patterns, suggesting that the CMF bundles formed separate agglomerated domains. The limited dispersion for contents above 7 wt % was related to thermodynamic instability of the prepared solutions, resulting in CMF phase separation before the microfibrils were rapidly sealed inside the PMMA fiber matrix at

solidification. Interestingly, both cellulose microfibrils and PMMA showed an improved thermal stability as long as the CMF was encapsulated as highly dispersed domains in the PMMA (up to 7 wt %). Increasing contents of CMF in electrospinning solutions (for a constant mass of PMMA polymer) resulted in a significant and gradual decrease in average fiber diameter of the biohybrid fibers. X-ray diffraction was demonstrated as an efficient tool for the evaluation of the CMF content in the hybrid fibers. The cellulose hybrid fibers could readily be aligned as yarns after collection on a static liquid medium. We envision that the microfibrils of cellulose have potential as an environmentally sound reinforcement agent for electrospun polymeric materials, in particular materials with demands to show biocompatibility such as in bioscaffolds and wound dressings but also in filters and membranes that require mechanical integrity.

Acknowledgment. The MAT2006-10261-C03 program is acknowledged as is the Knut & Alice Wallenberg Foundation for the fellowship in Micro/Nano Science (R.T.O.). J. Netrval is acknowledged for her assistance with microscopy sample preparation.

References and Notes

(1) Theron, S. A.; Zussman, E.; Yarin, A. L. *Polymer* **2004**, *45*, 2017–2030.
(2) Huang, Z.-M.; Zhang, Y.-Z.; Kotaki, M.; Ramakrishna, S. *Compos. Sci. Technol.* **2003**, *63*, 2223–2253.
(3) Zhou, F.-L.; Gong, R.-H.; Porat, I. *Polym. Int.* **2008**, *58*, 331–342.
(4) Huang, Z.-M.; Zhang, Y.-Z.; Kotaki, M.; Ramakrishna, S. *Compos. Sci. Technol.* **2003**, *63*, 2223–2253.
(5) Bergshoef, M. M.; Vancso, G. J. *Adv. Mater.* **1999**, *11*, 1362–1365.
(6) Schreuder-Gibson, H.; Gibson, P.; Senecal, K.; Sennett, M.; Walker, J.; Yeomans, W.; Tsai, P. *J. Adv. Mater.* **2002**, *34*, 44–55.
(7) Barhate, R. S.; Ramakrishna, S. *J. Membr. Sci.* **2007**, *296*, 1–8.
(8) Lui, H.; Kameoka, J.; Czaplewski, D. A.; Craighead, H. G. *Nano Lett.* **2004**, *4*, 671–675.
(9) Buchko, C. J.; Chen, L. C.; Shen, Y.; Martin, D. C. *Polymer* **1999**, *40*, 7397–7407.
(10) Zhou, Y. S.; Yang, D. Z.; Chen, X. M.; Xu, Q.; Lu, F. M.; Nie, J. *Biomacromolecules* **2008**, *9*, 349–354.
(11) Lee, K. H.; Kim, H. Y.; Khil, M. S.; Ra, Y. M.; Lee, D. R. *Polymer* **2003**, *44*, 1287–1294.
(12) Lee, K. H.; Kim, H. Y.; Ryu, Y. J.; Kim, K. W.; Choi, S. W. *J. Polym. Sci., Part B: Polym. Phys.* **2003**, *41*, 1256–1262.
(13) Ma, Z.; Kotaki, M.; Ramakrishna, S. *J. Membr. Sci.* **2006**, *272*, 179–187.
(14) Lee, K. H.; Kim, H. Y.; La, Y. M.; Lee, D. R.; Sung, N. H. *J. Polym. Sci., Part B: Polym. Phys.* **2002**, *40*, 2259–2268.
(15) Yang, F.; Both, S. K.; Yang, X.; Walboomers, X. F.; Jansen, J. A. *Acta Biomater.* **2009**, *5*, 3295–3304.
(16) Fang, J.; Lin, T.; Tian, W.; Sharma, A.; Wang, X. *J. Appl. Polym. Sci.* **2007**, *105*, 2321–2326.
(17) Zhang, Y. Z.; Venugopala, J.; Huang, Z.-M.; Lima, C. T.; Ramakrishna, S. *Polymer* **2006**, *47*, 2911–2917.
(18) Wang, X.; Zhang, K.; Zhu, M.; Hsiao, B. S.; Chu, B. *Macromol. Rapid Commun.* **2008**, *29*, 826–831.
(19) Dror, Y.; Salalha, W.; Khalfin, R. L.; Cohen, Y.; Yarin, A. L.; Zussman, E. *Langmuir* **2003**, *19*, 7012–7020.
(20) Katz, E. A.; Yarin, L.; Salalha, W.; Zussman, E. *J. Appl. Phys.* **2006**, *100*, 034313-1–034313-11.
(21) Hunley, M. T.; Pötschke, P.; Long, T. E. *Macromol. Rapid Commun.* **2009**, *30*, 2102–2106.
(22) Chen, D.; Liu, T.; Zhou, X.; Tjiu, W. C.; Hou, H. *J. Phys. Chem. B* **2009**, *113*, 9741–9748.
(23) Li, M.; Zhang, J.; Zhang, H.; Liu, Y.; Wang, C.; Xu, X.; Tang, Y.; Yang, B. *Adv. Funct. Mater.* **2007**, *17*, 3650–3656.
(24) Amiran, J.; Nicolosi, V.; Bergin, S. D.; Khan, U.; Lyons, P. E.; Coleman, J. N. *J. Phys. Chem. C* **2008**, *112*, 3519–3524.
(25) Blond, D.; Walshe, W.; Young, K.; Blighe, F. M.; Khan, U.; Almecija, D.; Carpenter, L.; McCauley, J.; Blau, W. J.; Coleman, J. N. *Adv. Funct. Mater.* **2008**, *18*, 2618–2624.
(26) Coleman, J. N.; Khan, U.; Blau, W. J.; Gun'ko, Y. K. *Carbon* **2006**, *44*, 1624–1652.
(27) Hsieh, Y. −C.; Yano, H.; Nogi, M.; Eichhorn, S. J. *Cellulose* **2008**, *15*, 507–513.
(28) Nishiyama, Y. *J. Wood Sci.* **2009**, *55*, 241–249.
(29) Iwamoto, S.; Kai, W.; Isogai, A.; Iwata, T. *Biomacromolecules* **2009**, *10*, 2571–2576.
(30) Hepworth, D. G.; Bruce, D. M. *J. Mater. Sci.* **2000**, *35*, 5861–5865.
(31) Mark, R. E. *Cell Wall Mechanics of Tracheids*; Yale University Press: New Haven, CT, 1967.
(32) Kroonbatenburg, L. M. J.; Kroon, J.; Northolt, M. G. *Polym. Commun.* **1986**, *27*, 290–292.
(33) Verlac, C.; Dedier, J. *J. Polym. Sci., Part A: Polym. Chem.* **1990**, *28*, 1171–1177.
(34) Rowland, S. P.; Roberts, E. J.; French, A. D. *J. Polym. Sci., Part A: Polym. Chem.* **1974**, *12*, 445–454.
(35) Habibi, Y.; Goffin, A. L.; Schiltz, N.; Duquesne, E.; Dubois, P.; Dufresne, A. *J. Mater. Chem.* **2008**, *18*, 5002–5010.
(36) Lönnberg, H.; Fogelström, L.; Berglund, L.; Malmström, E.; Hult, A. *Eur. Polym. J.* **2008**, *44*, 2991–2997.
(37) Kim, D.-Y.; Nishiyama, Y.; Kuga, S. *Cellulose* **2002**, *9*, 361–367.
(38) Nogi, M.; Abe, K.; Hanada, K.; Nakatsubo, F.; Ifuku, S.; Yano, H. *Appl. Phys. Lett.* **2006**, *89*, 233123.
(39) Hubbe, M. A.; Rojas, O. J.; Lucia, L. A.; Sain, M. *BioRes.* **2008**, *3*, 929–980.
(40) Nakagaito, A. N.; Yano, H. *Cellulose Nanocomposites: Processing, Characterization, and Properties*; ACS Symposium Series 938; American Chemical Society: Washington, DC, 2006; p 151.
(41) Udhardt, U.; Hesse, S.; Klemm, D. *Macromol. Symp.* **2005**, *223*, 201–212.
(42) Colvin, J. R. *Planta* **1980**, *149*, 97–107.
(43) Kohler, R.; Nebel, K. *Macromol. Symp.* **2006**, *244*, 97–106.
(44) Bledzki, A. K.; Reihmane, S.; Gassan, J. *J. Appl. Polym. Sci.* **1996**, *59*, 1329–1336.
(45) Abe, K.; Nakatsubo, F.; Yano, H. *Compos. Sci. Technol.* **2009**, *69*, 2434–2437.
(46) Bondeson, D.; Oksman, K. *Composites: Part A* **2007**, *38*, 2486–2492.
(47) Malainine, M. E.; Mahrouz, M.; Dufresne, A. *Compos. Sci. Technol.* **2005**, *65*, 1520–1526.
(48) Park, W.-I.; Kang, M.; Kim, H.-S.; Jim, H.-J. *Macromol. Symp.* **2007**, *249−250*, 289–294.
(49) Rojas, O. J.; Montero, G. A.; Habibi, Y. *J. Appl. Polym. Sci.* **2009**, *113*, 927–935.
(50) Kulshreshta, A. K.; Dweltz, N. E. *J. Polym. Sci.* (*Phys Ed.*) **1973**, *11*, 487–497.
(51) Hulta, E.-L.; Yamanaka, S.; Ishihara, M.; Sugiyama, J. *Carbohydr. Polym.* **2003**, *53*, 9–14.
(52) Iguchi, M.; Yamanaka, S.; Budhiono, A. *J. Mater. Sci.* **2000**, *35*, 261–270.
(53) Aulin, C.; Varga, I.; Claesson, P. M.; Wagberg, L.; Lindström, T. *Langmuir* **2008**, *24*, 2509–2518.
(54) Marchessault, R. H.; Morehead, F. F.; Walter, N. M. *Nature* **1959**, *184*, 632–633.
(55) Dong, X. M.; Kimura, T.; Revol, J. F.; Gray, D. G. *Langmuir* **1996**, *12*, 2076–2082.
(56) Thimm, J. C.; Burrit, D. J.; Sims, I. M.; Newman, R. H.; Ducker, W. A.; Melton, L. D. *Physiol. Plant.* **2002**, *116*, 164–171.
(57) Frey-Wyssling, A.; Mühlethaler, K. *Makromol. Chem.* **1963**, *62*, 25–30.
(58) Lai-Kee-Him, J.; Chanzy, H.; Müllers, M.; Putaux, J.-L.; Imai, T.; Bulone, V. *J. Biol. Chem.* **2002**, *277*, 36931–36939.
(59) Brown, R. M.; Willison, J. H. M.; Richardson, C. L. *Proc. Natl. Acad. Sci. U.S.A.* **1976**, *73*, 4565–4569.
(60) Klemm, D.; Schmauder, H.-P.; Heinze, T. In *Biopolymers*; Steinbüchel, A., Eds.; Wiley-VCH Verlag GmbH & Co.: Weinheim, Germany, 2003; Vol. *6*, pp 275.
(61) Nieduszynski, I.; Preston, R. D. *Nature* **1970**, *225*, 273–274.
(62) Tsekos, I.; Orologas, N.; Herth, W. *Phycologia* **1999**, *38*, 217–224.
(63) Ohad, I.; Danon, D. *J. Cell. Biol.* **1964**, *22*, 302–305.
(64) Ohad, I.; Mejzler, D. *J. Polym. Sci.: Part A* **1965**, *3*, 399–406.
(65) Elazzouzi-Hafraoui, S.; Nishiyama, Y.; Putaux, J.-L.; Heux, L.; Dubreuil, F.; Rochas, C. *Biomacromolecules* **2008**, *9*, 57–65.
(66) Azizi Samir, M. A. S.; Alloin, F.; Dufresne, A. *Biomacromolecules* **2005**, *6*, 612–626.
(67) Roman, M.; Winter, W. T. *Biomacromolecules* **2004**, *5*, 1671–1677.
(68) Kim, D.-Y.; Nishiyama, Y.; Wada, M.; Kuga, S. *Cellulose* **2001**, *8*, 29–33.

(69) Heux, L.; Dinand, E.; Vignon, M. R. *Carbohydr. Polym.* **1999**, *40*, 115–124.
(70) Pai, C.-L.; Óbice, M. C.; Rutledge, G. C. *Macromolecules* **2009**, *42*, 2102–2114.
(71) Arinstein, A.; Avrahami, R.; Zussman, E. *J. Phys. D: Appl. Phys.* **2009**, *42*, 015507–015513.
(72) Dror, Y.; Salalha, W.; Khalfin, R. L.; Cohen, Y.; Yarin, A. L.; Zussman, E. *Langmuir* **2003**, *19*, 7012–7020.
(73) Katz, E.; Yarin, A. L.; Salalha, W.; Zussman, E. *J. Appl. Phys.* **2006**, *100*, 034313-1–034313-11.
(74) Hunley, M. T.; Pötschke, P.; Long, T. E. *Macromol. Rapid Commun.* **2009**, *30*, 000–000.
(75) Kacir, L.; Narkis, M.; Ishai, O. *Polym. Eng. Sci.* **1975**, *15*, 525–532.
(76) Heyn, A. N. J. *J. Cell. Biol.* **1966**, *29*, 181–197.
(77) Lin, T.; Wang, H.; Wang, H.; Wang, X. *Nanotechnology* **2004**, *15*, 1375–1381.
(78) Pai, C.-L.; Boyce, M. C.; Rutledge, G. C. *Macromolecules* **2009**, *42*, 2102–2114.
(79) Sugiyama, J.; Voung, R.; Chanzy, H. *Macromolecules* **1991**, *24*, 4168–4175.
(80) Yamamoto, H.; Horii, F.; Odani, H. *Macromolecules* **1989**, *22*, 4130–4132.
(81) Wada, M.; Okano, T.; Sugiyama, J. *Cellulose* **1997**, *4*, 221–232.
(82) Wada, M.; Okano, T. *Cellulose* **2001**, *8*, 183–188.
(83) Hirai, A.; Tsuji, M.; Yamamoto, H.; Horii, F. *Cellulose* **1998**, *5*, 201–213.
(84) Smit, E.; Büttner, U.; Sanderson, D. *Polymer* **2005**, *46*, 2419–2423.
(85) Teo, W.-E.; Gopal, R.; Ramaseshan, R.; Fujihara, K.; Ramakrishna, S. *Polymer* **2007**, *48*, 3400–3405.
(86) Han, T.; Reneker, D. H.; Yarin, L. Y. *Polymer* **2007**, *48*, 6064–6076.
(87) Li, D.; Wang, Y. *Nano Lett.* **2003**, *3*, 1167–1171.
(88) Fennessey, S. F.; Farris, R. J. *Polymer* **2004**, *45*, 4217–4225.
(89) Katta, P.; Alessandro, M.; Ramsier, R. D.; Chase, G. G. *Nano Lett.* **2004**, *4*, 2215–2218.
(90) Sundaray, B.; Subramanian, V.; Natarajan, T. S.; Xiang, R. Z.; Chang, C. C.; Fann, W. S. *Appl. Phys. Lett.* **2004**, *84*, 1222–1224.
(91) Carnell, L. S.; Sioch, E. J.; Holloway, N. M.; Stephens, R. M.; Rhim, C.; Niklason, L. E.; Clark, R. L. *Macromolecules* **2008**, *41*, 5345–5349.
(92) Zussman, E.; Rittel, D.; Yarin, A. L. *Appl. Phys. Lett.* **2003**, *82*, 3958–3960.
(93) Theron, A.; Zussman, E.; Yarin, A. L. *Nanotechnology* **2001**, *12*, 384–390.
(94) Li, D.; Wang, Y.; Xia, Y. *Adv. Mater.* **2004**, *16*, 361–366.